Output irradiance of tapered lightpipes

Ivan Moreno

Unidad Academica de Fisica, Universidad Autonoma de Zacatecas, 98060 Zacatecas, Mexico (imoreno@fisica.uaz.edu.mx)

Received June 10, 2010; accepted July 9, 2010;
posted July 19, 2010 (Doc. ID 129840); published August 12, 2010

A light cone efficiently transports, distributes, and concentrates the incoming radiation. I derive a formula for the spatial irradiance (or illuminance) distribution at the exit aperture of a tapered light pipe. The theory is demonstrated by Monte Carlo ray-tracing for lightpipes with light-emitting diodes at the input face. The analysis is based on the addition of the radiation patterns of the multiple virtual sources that, as in a three-dimensional kaleidoscope, are seen through a tapered light tube. Given its explicit dependence on the structural and optical parameters, this analysis may be a useful tool in the development and application of light cones.

OCIS codes: 030.5620, 080.3685, 150.2950.

1. INTRODUCTION

In solid-state lighting, solar technology, and in other important fields a lightpipe is a very useful component [1–14]. Lightpipes or mixing rods are optical transmission elements that utilize reflection to reduce light losses and to distribute the radiation [12–14]. A tapered lightpipe also has the important property of concentrating light [12–14]. The input and output ends of a tapered rod have different sizes. If the output is larger than the input, a tapered lightpipe narrows the angular intensity distribution and increases the light-emitting area. In the opposite situation, when the exit aperture is smaller than the entrance, a tapered rod concentrates the light in a small illumination area and widens the angular intensity distribution. In this paper I focus on lightpipes whose exit face is larger than the entrance aperture.

In most applications a uniform illumination distribution is necessary [1,7–16]. To achieve a desired level of uniformity, several parameters of the mixing rod and the light source must be fitted. These tasks are usually performed via Monte Carlo ray-tracing, and most of the time the optimization is based on rules of thumb and designer experience. The optimization can be performed or assisted by analytic methods, because they provide a powerful conceptual framework and useful additional tools [2,3,8,10–17]. Calculating the output illumination distribution by means of a mathematical formula avoids the statistical noise of ray-tracing, and allows the calculation of derivatives and integrals. In this paper, I analytically compute the spatial irradiance distribution of a tapered lightpipe with rectangular cross section (Fig. 1). The formulas are valid for both solid and hollow lightpipes. These equations may be a useful design tool for experts of different fields because light cones are easy to manufacture and suitable for many applications.

The first analytical treatment was reported by Chen *et al.* for a "straight" lightpipe with square cross section and with one point source in the middle of the input [17]. They viewed the lightpipe as a kaleidoscope, and they superimposed at the output sub-regions of the irradiance distribution that would be obtained without using a mixing rod. A similar approach is the "images method." If one looks through the lightpipe toward the light source, multiple images of the source can be observed as in a kaleidoscope. The "images method" adds the illumination distributions of the multiple virtual sources to calculate the output distribution of the mixing rod. The idea is equivalent to that of Chen *et al.*, but facilitates some calculations. Recently, based on this idea, an analytic approach was reported by Cheng and Chern for a "straight" lightpipe with rectangular cross section and with multiple point sources at the entrance [11]. Moreover, they showed the wide range of design possibilities when the light source is an array of light-emitting diodes (LEDs). Just think about the millions of possible arrangements of images that can be seen through a kaleidoscope.

When using the images method, it is necessary to know the location of each virtual source. For a "straight" rod, these images spread over a plane (two-dimensional surface) [11]. However, for a tapered lightpipe the images distribute over a three-dimensional (3D) surface. This fact immediately provokes a question: what is the shape of this mesh of virtual sources?

The images are produced by the lightpipe walls, which behave as mirrors. The multiple images seen between two mirrors that sit at an angle to each other lie over a circle [18]. Using a tunnel diagram [13], it is easy to show that the center of that circle is located at the imaginary intersection of the mirrors. A tapered lightpipe can be viewed as an assembly of four mirrors, in which each pair sits an angle to each other. Therefore, a 3D tunnel construction shows that the array of images lies over a sphere (Fig. 2). The center of the sphere is at the virtual intersection of the four walls of the lightpipe. If the cross section is not a square but a rectangle, images spread over a section of a torus [Fig. 2(c)]. A toroidal surface has two radii of curvature. Each of these centers of curvature is located in the virtual intersection of each pair of lightpipe walls. In the simplest case, when two of the walls are parallel, the virtual images rest on a cylinder (a limiting case of a torus).

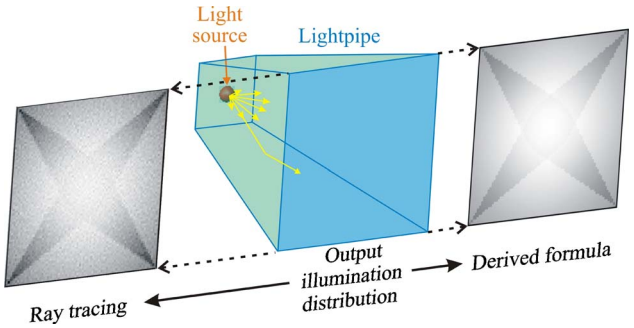

Fig. 1. (Color online) Diagram of a tapered lightpipe with a light source in the entrance. This figure also shows the irradiance (or illuminance) spatial distribution that would be measured or projected in a screen at the exit aperture of the lightpipe.

2. ANGULAR POSITION OF VIRTUAL IMAGES

For implementing the images method, it is necessary to know the location of each virtual source. The exact position of the images in a "straight" lightpipe is a multiple of the distance between the source and each wall, i.e., the ijth image along x and y directions is located at [11,17]

$$x_{si} = i\mathrm{a} + (-1)^i x_s, \quad y_{sj} = j\mathrm{b} + (-1)^j y_s,$$

where a and b are the width and height of the tube cross section, respectively. (x_s, y_s) are the Cartesian coordinates of the sth light source.

However, because the walls of a tapered lightpipe are inclined, this task is simplified by using angles instead of distances. The images are shifted at a multiple of the angle between the light source and each wall. In other words, the ijth image is displaced along x and y directions [Fig. 3(a)] by

$$\alpha_{si} = i\Delta_x + (-1)^i \arctan(x_s/R_x),$$

$$\alpha_{sj} = j\Delta_y + (-1)^j \arctan(y_s/R_y), \tag{1}$$

where (x_s, y_s) are the Cartesian coordinates of the sth source [Fig. 3(b)]. R_x and R_y are the two radii of curvature of the array of images from a source in the middle of the entrance ($x_s=0$, $y_s=0$), and along x and y directions, i.e., $R_x=[d_x H/(D_x-d_x)]$ and $R_y=[d_y H/(D_y-d_y)]$. All these coordinates and parameters are illustrated in Fig. 3. Δ_x and Δ_y are the angles between each pair of walls along x and y directions, respectively, i.e., $\Delta_x = 2\arctan[(D_x-d_x)/2H]$ and $\Delta_y = 2\arctan[(D_y-d_y)/2H]$. H is the lightpipe length, $d_x \times d_y$ is the input size, and the output size is $D_x \times D_y$ [Fig. 3(c)]. The notation used in the paper is listed in Appendix A.

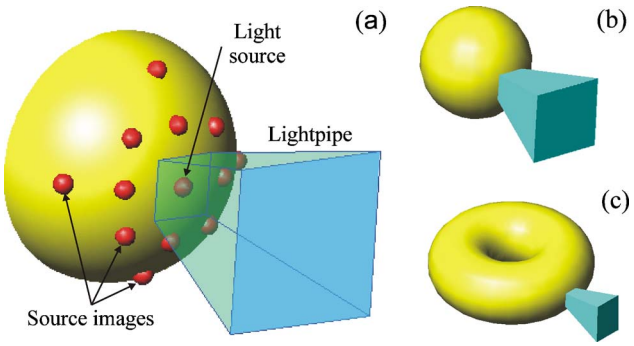

Fig. 2. (Color online) (a) Schematic that depicts what is viewed from the output of the lightpipe, an array of virtual images of the light source. (b), (c) 3D locus of the virtual sources of a lightpipe with square and rectangular cross section.

The Cartesian coordinates of the ijth image are deduced by using a 3D tunnel diagram. It must be noted that each pair of mirrors not only rotates every image through a circle, but also rotates the images of the other (perpendicular) pair of mirrors. This key point indicates that, in general, the image placement is not the result of a simple rotation along the x and y axes. It is the result of consecutive rotations along rotated axes. Therefore, the Cartesian coordinates of the ijth image are obtained by using spherical trigonometry. These coordinates are introduced in the next section after the irradiance formula.

3. IRRADIANCE SPATIAL DISTRIBUTION

The output irradiance or illuminance ($\mathrm{W/m^2}$ or $\mathrm{lm/m^2}$) is the power distribution that illuminates the exit face of the lightpipe [Fig. 3(b)]. To compute the output irradiance, I model the lightpipe as an array of light sources composed of real and virtual emitters. In this way, the irradiance distribution E_L is the superposition of irradiances due to each real and image source, i.e., it is the sum of the irradiances due to the "sources" that are visible from the output:

$$E_L = \sum E_{sources} + \sum E_{images}. \tag{2}$$

As usually happens with LEDs the source size is small, and the spatial irradiance distribution of each source can be approximated by [19,20]

$$E_s(X,Y,Z) = \frac{Z}{(X^2+Y^2+Z^2)^{3/2}} I_s[\theta_s(X,Y,Z)]. \tag{3}$$

It is the irradiance over every point (X,Y) on a plane at distance Z from the light source. Angle θ_s is the view angle of the source, subtended by an illuminated point (X,Y). Here $I_s(\theta)$ is the radiant (or luminous) intensity (W/sr or lm/sr) of the source, which can be easily modeled and measured for most LEDs [19,20]. If the intensity is simulated with cosine functions (e.g., $I_s(\theta)=I_0\cos\theta$ for Lambertian LEDs), it must be made zero at angles larger than 90 °. For example, $I_s(\theta)=I_0(\theta)\cos\theta$ for Lambertian LEDs, where $I_0(\theta \leqslant 90°)=I_0$ and $I_0(\theta > 90°)=0$. In addition, note that a lightpipe with an extended light source in the input can be simulated if an appropriate source model is used instead of Eq. (3).

If a light source is located in (x_s, y_s, z_s), or in general if the ijth image of the sth source is located in $(x_{sij}, y_{sij}, z_{sij})$, E_s must be shifted, i.e., $E_s(x-x_{sij}, y-y_{sij}, z-z_{sij})$. This is the irradiance over every point (x,y) on the output plane at distance z from the lightpipe input due to a source located in $(x_{sij}, y_{sij}, z_{sij})$. The same shift happens with the view angle, i.e., $\theta_s(x-x_{sij}, y-y_{sij}, z-z_{sij})$. For simplicity of notation I write it as $\theta_{sij}(x,y,z)$; the particular value $\theta_{s(-1)0}$ is shown in Fig. 3(a). In general, this angle is

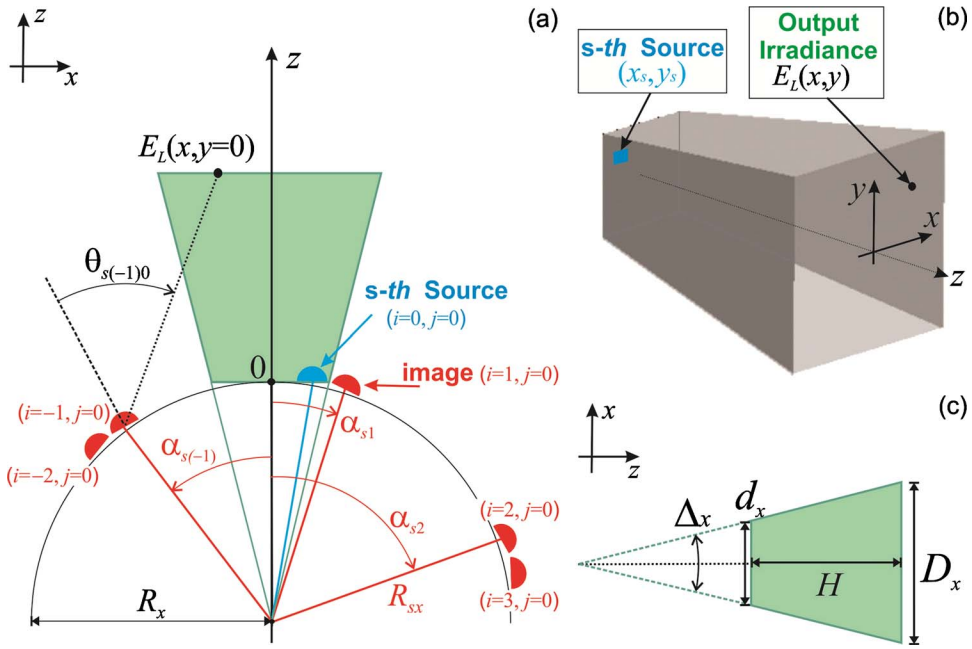

Fig. 3. (Color online) Geometry and coordinate system for calculation of irradiance distribution. (a) Angular shift along x-direction. (b) Cartesian coordinates of the sth source at the entrance plane. (c) Some lightpipe parameters.

$$\theta_{sij}(x,y,z) = \arccos\left[\frac{\vec{n}_{ij}\cdot(\vec{r}-\vec{r}_{sij})}{|\vec{n}_{ij}||\vec{r}-\vec{r}_{sij}|}\right]. \tag{4}$$

Here $\vec{r}$ is the location vector of the output point (x,y,z), $\vec{r}_{sij}$ is the location vector of the ijth image of the sth source, and $\vec{n}_{ij}$ is the normal vector of the ijth image of the input plane.

If the array of images is a sphere of radius R, Eq. (4) can be simplified to

$$\theta_{sij}(x,y,z) = \arccos\left[\frac{x_{0ij}(x-x_{sij})+y_{0ij}(y-y_{sij})+(z_{0ij}+R)(z-z_{sij})}{R\sqrt{(x-x_{sij})^2+(y-y_{sij})^2+(z-z_{sij})^2}}\right], \tag{5}$$

where $(x_{0ij},y_{0ij},z_{0ij})$ is the location of the ijth image of a source located in the center of the input face $(x_s=0, y_s=0)$, and $R=[dH/(D-d)]$ for a square cross section lightpipe. For Eq. (5), the origin of the coordinate system is located at the center of the entrance [Fig. 3(a)].

On the other hand, if the array of images is a cylinder of radius R, Eq. (4) becomes—if the cylinder axis is along the y-direction—

$$\theta_{sij}(x,y,z) = \arccos\left[\frac{x_{0i}(x-x_{si})+(z_{0i}+R)(z-z_{si})}{R\sqrt{(x-x_{si})^2+(y-y_{sj})^2+(z-z_{si})^2}}\right], \tag{6a}$$

and if the cylinder axis is the x axis

$$\theta_{sij}(x,y,z) = \arccos\left[\frac{y_{0j}(y-y_{sj})+(z_{0j}+R)(z-z_{sj})}{R\sqrt{(x-x_{si})^2+(y-y_{sj})^2+(z-z_{sj})^2}}\right]. \tag{6b}$$

Here (x_{0i},y_{0j},z_{0i}) and (x_{0i},y_{0j},z_{0j}) are the location coordinates of the ijth image of a central source $(x_s=0, y_s=0)$ in Eqs. (6a) and (6b), respectively.

Let me now turn to the equations of irradiance distribution for the three basic lightpipe geometries: square cross section (sphere of images), rectangular cross section (torus of images), and (when two walls are parallel) cylinder of images. I begin with the simplest case, a lightpipe with only two tapered walls.

A. Two Walls are Parallel: Cylinder of Images

If only two walls are tapered it means that $d_x=D_x$ or $d_y=D_y$. As I explained before, a 3D tunnel construction shows that the array of images lies over a cylinder.

The output irradiance distribution E_L is the superposition of irradiances due to each source, and virtually due to each image. Therefore, for an array of K sources in the input, the irradiance distribution at the lightpipe output is, if $d_y=D_y$,

$$E_L(x,y) = \sum_{s=1}^{K}\sum_{i=-N_{-x}}^{N_x}\sum_{j=-N}^{N}\rho^{|i|+|j|}E_s(x-x_{si},y-y_{sj},H-z_{si}), \tag{7a}$$

and, if $d_x=D_x$,

$$E_L(x,y) = \sum_{s=1}^{K}\sum_{i=-N}^{N}\sum_{j=-N_{-y}}^{N_{+y}}\rho^{|i|+|j|}E_s(x-x_{si},y-y_{sj},H-z_{sj}), \tag{7b}$$

where $-D_x/2\leqslant x\leqslant D_x/2$ and $-D_y/2\leqslant y\leqslant D_y/2$. For simplicity, the origin of the coordinate system is placed at the center of the input face [Fig. 3(a)], and then the output plane is at $z=H$. $N_{\pm x}$ is the number of images that are visible along the $\pm x$ direction from the lightpipe output, and $N_{\pm y}$ along the $\pm y$ direction. These numbers are given by Eqs. (B1) and (B2) in Appendix B. Number N is given by Eqs. (B3) and (B4) in Appendix B. $E_s(x,y,z)$ is the irradiance distribution produced by the sth light source. If the source size is small, E_s can be represented by Eq. (3), and

the view angle θ_{sij} is given by Eq. (6a) or (6b). The irradiance of each image is weighted by the $(|i|+|j|)$th power of the reflectivity ρ of the side walls of the lightpipe. For hollow lightpipes this is the reflectivity of the metal coating, which in the case of aluminum is about 90% in the visible spectrum. For solid lightpipes, the reflection is mostly determined by total internal reflection, which is for practical purposes 99.9% [7]. However, the reflectivity can be low near the lightpipe input because the angle of incidence of rays at the walls close to the source can be smaller than the critical angle. This can be avoided by adding a reflecting coating in one small part of the walls, close to the input.

The Cartesian coordinates of the ijth image of the sth light source are, if $d_x=D_x$,

$$x_{si}=id_x+(-1)^i x_s,\quad y_{sj}=R_{sy}\sin\alpha_{sj},\quad z_{sj}=R_{sy}\cos\alpha_{sj}-R, \tag{8}$$

and, if $d_y=D_y$,

$$x_{si}=R_{sx}\sin\alpha_{si},\quad y_{sj}=jd_y+(-1)^j y_s,\quad z_{si}=R_{sx}\cos\alpha_{si}-R. \tag{9}$$

Here $R_{sx}=(x_s^2+R^2)^{1/2}$ and $R_{sy}=(y_s^2+R^2)^{1/2}$. The angular coordinates α_{si} and α_{sj} are given by Eq. (1), with $R_x=R$ or $R_y=R$.

In order to close this section, Eq. (7a) is used in the examples illustrated in Figs. 4 and 5. These figures show the irradiance distribution at the output of a hollow tapered rod with parameters: $d_x=3$, $d_y=3$, $D_x=6$, $D_y=d_y$, $H=4$, $\rho=0.9$. Figure 4 is for a lightpipe with one Lambertian LED located at the center of the input face, i.e., in $(x_s=0, y_s=0)$. For illustrative purposes, we model the LED as a point source, i.e., we use Eq. (3) for this and the following figures. In Fig. 5 the LED is placed at one corner of the input face $(x_s=1.5, y_s=1.5)$. For comparison purposes, both figures include the irradiance pattern generated with Monte Carlo ray-tracing. The match between theory and ray-tracing indicates that Eqs. (7a) and (7b) are exact solutions.

B. Square Cross Section: Sphere of Images

The shape of the input and output faces is squared if $d_x=d_y=d$ and $D_x=D_y=D$. For this lightpipe geometry the array of source images is a sphere [Fig. 2(b)].

For a cylinder of images the solution was relatively easy, but the square cross section adds an additional complication. As an observer views the sphere of images through the lightpipe, each image can be seen only

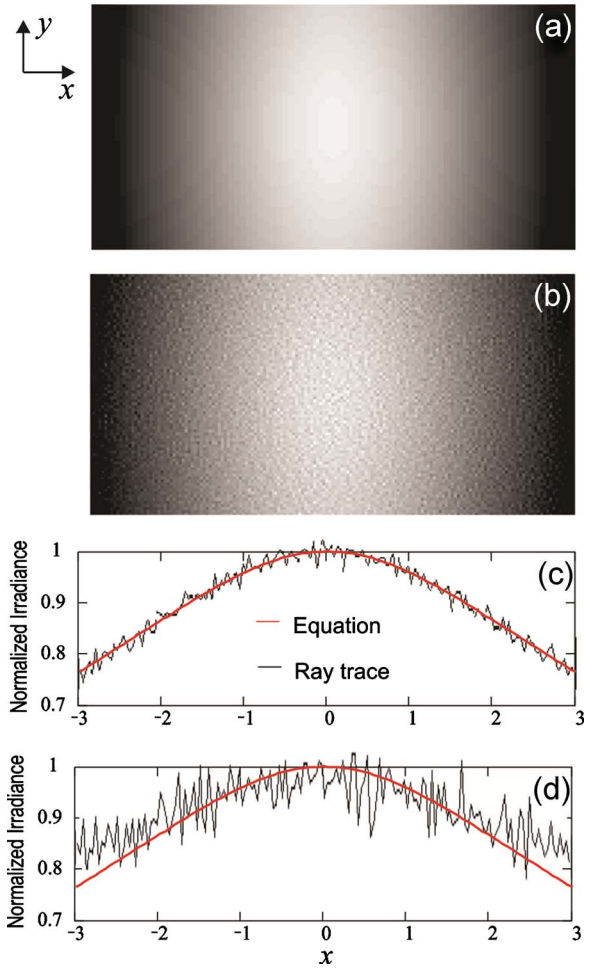

Fig. 4. (Color online) Irradiance distribution at the output of a hollow tapered rod with two parallel walls ($d_x=3$, $d_y=3$, $D_x=6$, $D_y=d_y$, $H=4$, $\rho=0.9$). One Lambertian LED is placed at the center of the input face. (a) Irradiance pattern obtained with Eq. (7a) and (7b). (b) Irradiance pattern generated with ray-tracing using 10^7 rays. (c) Detailed comparison between (a) and (b) along $x-$ direction and $y=0$. (d) Also compares the irradiance distributions but with only 10^6 rays.

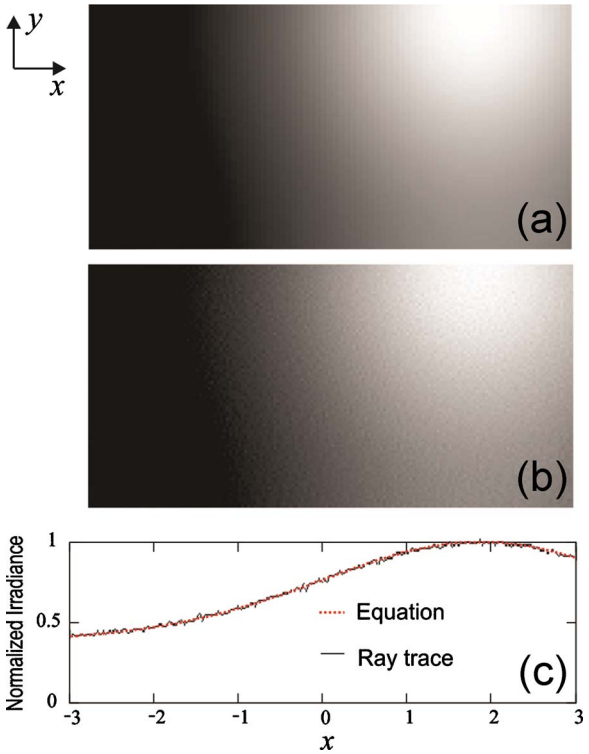

Fig. 5. (Color online) Output irradiance distribution of a hollow tapered rod with two parallel walls ($d_x=3$, $d_y=3$, $D_x=6$, $D_y=d_y$, $H=4$, $\rho=0.9$). One Lambertian LED is placed at one corner of the input face $(x_s=1.5, y_s=1.5)$. (a) Irradiance pattern obtained with Eq. (7a) and (7b). (b) Irradiance pattern generated with ray-tracing, using 10^7 rays. (c) Detailed comparison between (a) and (b) along $x-$ direction and $y=0$.

through a specific wall or through a group of virtual walls. The result is a set of windows allowing visualization of each image source rather than a virtual space freely showing all image sources (see Fig. 6). The problem is that the exact position of every source depends on the observation point. Even more, at particular places some image points are not visible from the output. The exact solution seems to be complex. To overcome such difficulty, I simplify this multiple window effect by taking into account only the main windows, i.e., by considering only the four real walls instead of all virtual walls.

As stated before, the output irradiance distribution is the sum of the irradiance distribution from each image source. Now, the array of virtual sources is partitioned into two sub-arrays and their contributions are added separately. The idea is that a pupil function W simulates the window effect for the four lateral walls.

Therefore, for an array of K sources in the input, the irradiance distribution at the lightpipe output ($z=H$) is

$$E_L(x,y)=\sum_{s=1}^{K}\sum_{i=-N_{-x}}^{N_{+x}}\sum_{j=-N_{-y}}^{N_{+y}}\rho^{|i|+|j|}h_{ij}[W1_{sij}E_s(x-x1_{sij},y-y1_{sj},H-z1_{sij})+W2_{sij}E_s(x-x2_{si},y-y2_{sij},H-z2_{sij})], \tag{10}$$

where $-D/2\leqslant x,y\leqslant D/2$. The number of images that are visible from the lightpipe output, $N_{\pm x}$ and $N_{\pm y}$, are given by Eqs. (B1) and (B2) in Appendix B. E_s is the irradiance distribution produced by the sth light source. If the source size is small, E_s can be represented by Eq. (3). The view angle θ_{sij} is given by Eq. (5), where ($x_{sij}=x1_{sij}$, $y_{sij}=y1_{sj}$, $z_{sij}=z1_{sij}$) for the first sub-array of images, and ($x_{sij}=x2_{si}$, $y_{sij}=y2_{sij}$, $z_{sij}=z2_{sij}$) for the second sub-array.

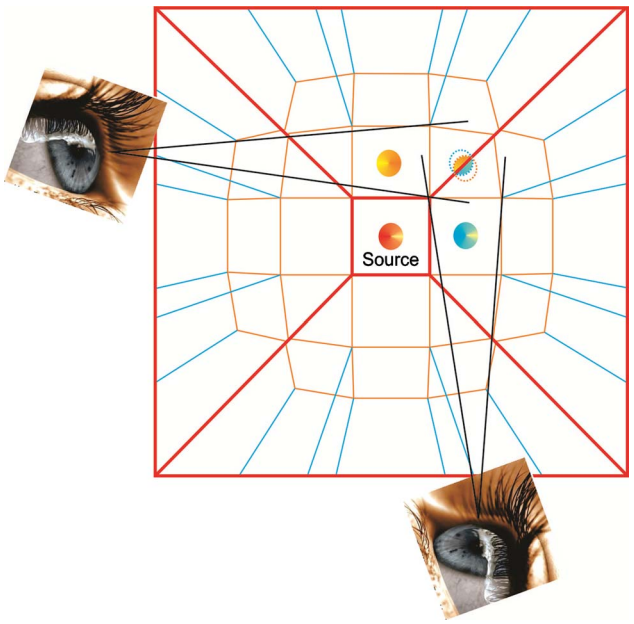

Fig. 6. (Color online) Virtual windows effect: As an observer views the sphere of images through the lightpipe, each image can be seen only through a specific wall or set of virtual walls. Dark (red online) lines show the four primary windows, light (blue online) lines the secondary virtual windows.

The irradiance of each image is weighted by the $(|i|+|j|)$th power of the reflectivity ρ of the side walls of the lightpipe. The term h_{ij} is a simple function that helps to make Eq. (10) a compact expression; it is $h_{00}=1/2$ and $h_{ij}=1$ for all other values of ij. For example, it can be $h_{ij}=1/[2-A(|i|+|j|)]$, where $A(0)=0$ and $A(\ell)=1$ for all other values of ℓ.

The coordinates of the ijth image of the sth light source that are seen through the pair of walls 1 (along the x-direction), are

$$x1_{sij}=R_s(x_s,A_jy_s)\cos(A_j\alpha_{sj})\sin\alpha_{si},$$

$$y1_{sj}=R_s(A_jx_s,y_s)\sin\alpha_{sj},$$

$$z1_{sij}=R_s(x_s,A_jy_s)\cos(A_j\alpha_{sj})\cos\alpha_{si}-R, \tag{11}$$

and for the other two windows are

$$x2_{si}=R_s(x_s,A_iy_s)\sin\alpha_{si},$$

$$y2_{sij}=R_s(A_ix_s,y_s)\cos(A_i\alpha_{si})\sin\alpha_{sj},$$

$$z2_{sij}=R_s(A_ix_s,y_s)\cos(A_i\alpha_{si})\cos\alpha_{sj}-R, \tag{12}$$

where $R_s(x_s,y_s)=(x_s^2+y_s^2+R^2)^{1/2}$. The function A_ℓ is a unitary function, i.e., it is $A_0=0$ and $A_\ell=1$ for all other values of ℓ. The angular coordinates α_{si} and α_{sj} are given by Eq. (1).

Window functions are defined as

$$W1_{sij}=\begin{Bmatrix}1 & if & V1_{sij}\geqslant 0\\ 0 & if & V1_{sij}<0\end{Bmatrix},\quad \text{and}$$

$$W2_{sij}=\begin{Bmatrix}1 & if & V2_{sij}\geqslant 0\\ 0 & if & V2_{sij}<0\end{Bmatrix} \tag{13}$$

where

$$V1_{sij}=Sign(i)Sign(j)\{x1_{sij}[(z+R)C_j-yH]+y1_{sj}[xH-(z+R)C_i]+(z1_{sij}+R)[yC_i-xC_j]\}, \tag{14a}$$

$$V2_{sij}=-Sign(i)Sign(j)\{x2_{si}[(z+R)C_j-yH]+y2_{sij}[xH-(z+R)C_i]+(z2_{sij}+R)[yC_i-xC_j]\}. \tag{14b}$$

Here $C_\ell=0.5(D\text{-}d)Sign(\ell)$. Function $Sign$ gives three possible values, i.e., $Sign(0)=0$, $Sign(-|\ell|)=-1$, and $Sign(|\ell|)=+1$.

In order to illustrate this analysis, Eq. (10) is used in the examples shown in Figs. 7 and 8. These figures show the irradiance distribution at the output of a hollow tapered rod. For comparison purposes, both figures include the irradiance pattern generated with Monte Carlo ray-tracing. Parameters in Fig. 7 are: $d=3$, $D=6$, $H=4$, $\rho=0.9$. This figure shows the irradiance pattern for a lightpipe with one Lambertian LED located at four different locations in the input face. It must be noted that Eq. (10) is very accurate when the source is placed near the optical axis [Fig. 7(a)], but it is not exact when the light source is near a corner [Fig. 7(d)]. The accuracy in the cor-

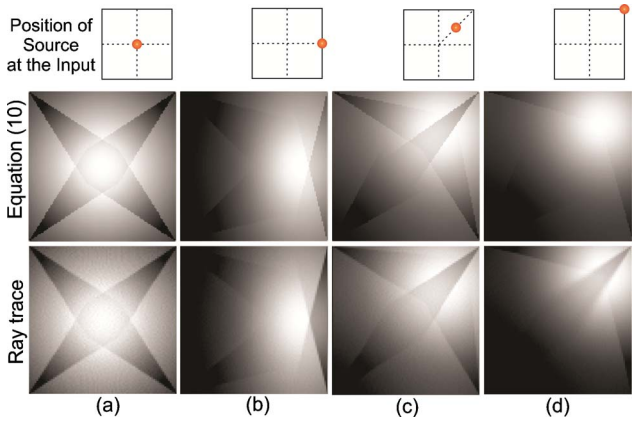

Fig. 7. (Color online) Output irradiance distribution of a square cross section tapered rod ($d=3$, $D=6$, $H=4$, $\rho=0.9$). One Lambertian LED is placed at different places of the input face. (a) LED is located at the center of the entrance ($x_s=0, y_s=0$). (b) LED is placed at ($x_s=1.5, y_s=0$). (c) LED is placed at ($x_s=0.75, y_s=0.75$). (d) LED is placed at one corner of the input face ($x_s=1.5, y_s=1.5$). The ray-tracing uses 10^7 rays.

ners can be improved if the effect of secondary windows is incorporated in the model (a task that opens a challenge for further research). Parameters in Fig. 8 are: $d=3$, $D=6$, $H=18$, $\rho=0.9$. This figure shows the effect of many windows because the lightpipe is long, and so many images are generated. It can be seen that secondary virtual windows are responsible for fine details in the irradiance pattern.

C. Rectangular Cross Section: Torus of Images

The shape of the input and output faces is rectangular if $d_x \neq d_y$ and $D_x \neq D_y$. For this lightpipe geometry the array of source images is a torus [Fig. 2(c)].

As I explained in Subsection 3.B, there is a set of windows limiting the visualization of each image source. Once again, to overcome such difficulty, the multiple window effect is simplified by taking into account only the main windows, i.e., by considering only the four real walls instead of all virtual walls.

The output irradiance distribution is the sum of the irradiance distribution from each image source. Once more, the array of virtual sources is partitioned into two sub-

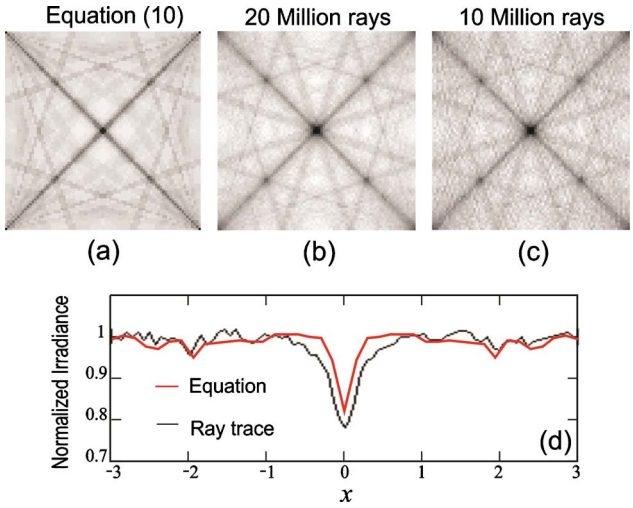

Fig. 8. (Color online) Output irradiance distribution of a square cross section tapered rod ($d=3$, $D=6$, $H=18$, $\rho=0.9$). One Lambertian LED is placed at the center of the input face. (a) Irradiance pattern obtained with Eq. (10). (b) Irradiance pattern generated with ray-tracing using 2×10^7 rays. (c) Irradiance pattern by using 10^7 rays. (d) Detailed comparison between (a) and (b) along x–direction and $y=0$.

arrays and their contributions are added separately. A pupil function W simulates the window effect for the four windows. Therefore, for an array of K sources in the input, the irradiance distribution at the lightpipe output ($z=H$) is

$$E_L(x,y) = \sum_{s=1}^{K} \sum_{i=-N_{-x}}^{N_{+x}} \sum_{j=-N_{-y}}^{N_{+y}} \rho^{|i|+|j|} h_{ij}[W1_{sij} E_s(x - x1_{sij}, y - y1_{sj}, H - z1_{sij}) + W2_{sij} E_s(x - x2_{si}, y - y2_{sij}, H - z2_{sij})]. \quad (15)$$

Note that this function is in fact Eq. (10), but it is a function of different parameters. Here $-D_x/2 \leqslant x \leqslant D_x/2$ and $-D_y/2 \leqslant y \leqslant D_y/2$. The number of images that are visible from the lightpipe output, $N_{\pm x}$ and $N_{\pm y}$, are given by Eqs. (B1) and (B2) in Appendix B. E_s is the irradiance distribution produced by the sth light source. If the source size is small, the irradiance can be represented by Eq. (3). The view angle θ_{sij}, for the first sub-array of images, is

$$\theta_{sij}(x,y,z) = \arccos\left[\frac{X1_{0ij}(x - x1_{sij}) + Y1_{0j}(y - y1_{sj}) + Z1_{0ij}(z - z1_{sij})}{\sqrt{X1_{0ij}^2 + Y1_{0j}^2 + Z1_{0ij}^2}\sqrt{(x - x1_{sij})^2 + (y - y1_{sj})^2 + (z - z1_{sij})^2}}\right], \quad (16a)$$

where $X1_{0ij} = x1_{0ij} - (R_x - R_y)\sin\alpha_{0i}$, $Y1_{0j} = y1_{0j}$, and $Z1_{0ij} = z1_{0ij} + R_x - (R_x - R_y)\cos\alpha_{0i}$. Here $(x1_{0ij}, y1_{0j}, z1_{0ij})$ is the location of the ijth image (through the window pair 1) of a source located in the center of the input face ($x_s=0$, $y_s=0$). Similarly, the view angle for sub-array 2 is

$$\theta_{sij}(x,y,z) = \arccos\left[\frac{X2_{0i}(x - x2_{si}) + Y2_{0ij}(y - y2_{sij}) + Z2_{0ij}(z - z2_{sij})}{\sqrt{X2_{0i}^2 + Y2_{0ij}^2 + Z2_{0ij}^2}\sqrt{(x - x2_{si})^2 + (y - y2_{sij})^2 + (z - z2_{sij})^2}}\right], \quad (16b)$$

where $X2_{0i}=x2_{0i}$, $Y2_{0ij}=y2_{0ij}-(R_y-R_x)\sin\alpha_{0j}$, and $Z2_{0ij}=z2_{0ij}+R_y-(R_y-R_x)\cos\alpha_{0j}$.

The irradiance of each image is weighted by the $(|i|+|j|)$th power of the reflectivity ρ of the side walls of the lightpipe. Term h_{ij} is a simple function that helps to make Eq. (15) compact; it is $h_{00}=1/2$ and $h_{ij}=1$ for all other values of ij.

The coordinates of the ijth image of the sth light source that are seen along the x-direction through the pair 1 of walls are

$$x1_{sij}=(R_{si}-R_{sj})\sin\alpha_{si}+R_{sj}\cos(A_j\alpha_{sj})\sin\alpha_{si},$$

$$y1_{sj}=R'_{sj}\sin\alpha_{sj},$$

$$z1_{sij}=(R_{si}-R_{sj})\cos\alpha_{si}+R_{sj}\cos(A_j\alpha_{sj})\cos\alpha_{si}-R_x, \tag{17a}$$

and along the y-direction, through pair 2 are

$$x2_{si}=R'_{si}\sin\alpha_{si},\quad y2_{sij}=(R_{sj}-R_{si})\sin\alpha_{sj}+R_{si}\cos(A_i\alpha_{si})\sin\alpha_{sj},$$

$$z2_{sij}=(R_{sj}-R_{si})\cos\alpha_{sj}+R_{si}\cos(A_i\alpha_{si})\cos\alpha_{sj}-R_y. \tag{17b}$$

Here $R_{si}=(A_ix_s^2+y_s^2+R_x^2)^{1/2}$, $R'_{si}=(x_s^2+A_iy_s^2+R_x^2)^{1/2}$, $R_{sj}=(x_s^2+A_jy_s^2+R_y^2)^{1/2}$, and $R'_{sj}=(A_jx_s^2+y_s^2+R_y^2)^{1/2}$. Function A_ℓ is a unitary function, i.e., it is $A_0=0$ and $A_\ell=1$ for all other values of ℓ. The angular coordinates α_{si} and α_{sj} are given by Eq. (1).

Window functions are defined as:

$$Wn_{sij}=\begin{Bmatrix}1 & if & Vn_{sij}\geq 0\\ 0 & if & Vn_{sij}<0\end{Bmatrix},\quad n=1,2 \tag{18}$$

where

$$Vn_{sij}=(-1)^{n+1}Sign(i)Sign(j)[Xn_{sij}(zC_j-Y_jH)+Yn_{sj}(X_iH-zC_i)+zn_{sij}(Y_jC_i-X_iC_j)],\quad n=1,2 \tag{19}$$

Here $C_i=0.5(D_x\text{-}d_x)Sign(i)$ and $C_j=0.5(D_y\text{-}d_y)Sign(j)$. And $Xn_{sij}=xn_{sij}-0.5d_xSign(i)$, $Yn_{sij}=yn_{sij}-0.5d_ySign(j)$, $X_i=x-0.5d_xSign(i)$, and $Y_j=y-0.5d_ySign(j)$. Function $Sign$ gives three possible values: $Sign(0)=0$, $Sign(-|\ell|)=-1$, and $Sign(|\ell|)=+1$.

Figure 9 illustrates this subsection. This figure shows the irradiance distribution at the output of a hollow tapered rod with one Lambertian LED located in the central point. For comparison purposes, the irradiance pattern generated with Monte Carlo ray-tracing is included. Parameters in Fig. 9 are $d_x=3$, $d_y=4$, $D_x=6$, $D_y=7$, $\rho=0.9$.

4. SUMMARY

In summary, I derived a formula for the irradiance distribution of a tapered lightpipe that explicitly depends on the structural and optical parameters. Three equations are reported for the three possible lightpipe geometries: square cross section, rectangular cross section, and two parallel walls. These formulas were obtained by adding the radiation patterns of the multiple virtual sources that, as in a kaleidoscope, are seen through the lightpipe. The analysis was verified by Monte Carlo ray-tracing.

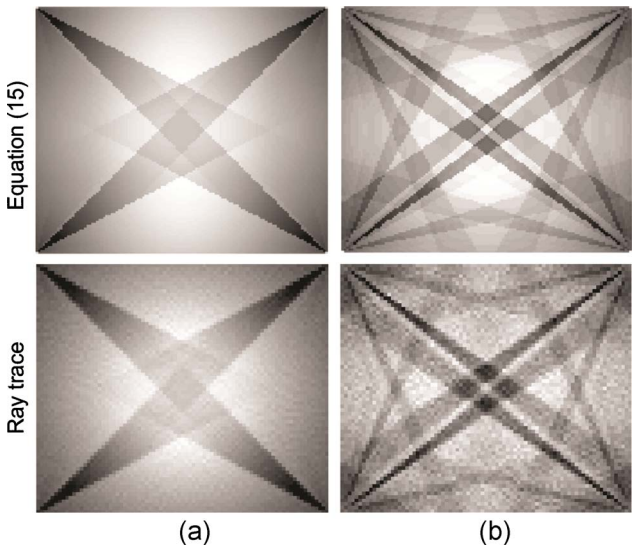

Fig. 9. (Color online) Irradiance distribution at the exit face of a rectangular cross section tapered rod, where the parameters are $d_x=3$, $d_y=4$, $D_x=6$, $D_y=7$, and $\rho=0.9$. One Lambertian LED is placed at the center of the input face. Figure shows the irradiance pattern obtained with both Eq. (15) and ray-tracing for (a) one tube with length $H=5$, (b) a tube with length $H=10$. The ray-tracing uses 10^7 rays.

Further research and applications of this analysis include: (A) A study of tapered lightpipes with polygonal cross sections, e.g., a hexagonal cross-section. (B) Determination of a precise formula, when the source is located in the corner, by considering secondary windows. (C) Optimization of illumination uniformity and color mixing, e.g., by finding the optimal source locations when using an array of LEDs as the primary source. A simple optimization method can find the illumination uniformity condition of a spherical array of LEDs [21]. (D) A tolerance analysis, e.g., the effect of variations in the radiation pattern shape of the light source [22]. (E) Analysis of "smart" lightpipes using LED arrays. There are millions of possible irradiance patterns that can be adaptively generated by individually modulating each LED [23]. (F) Analysis of a solar concentrator, i.e., a tapered lightpipe with the output face smaller than the input face. In this case the virtual sources point toward the center of the locus of images (cylinder, sphere, or torus), and then a different derivation is required, e.g., changing the signs of some equations is necessary.

APPENDIX A: NOTATION

E_L	Irradiance at the exit aperture of the lightpipe
E_s	Irradiance of the sth source placed at entrance of lightpipe
ρ	Reflectance of internal walls of the lightpipe
$N_{\pm x}(N_{\pm y})$	Number of visible images along $\pm x(\pm y)$ direction
K	Number of real light sources

(x,y)	Cartesian coordinates of a point in the output plane
(x_s,y_s)	Cartesian coordinates of the *sth* source placed at entrance aperture
$(x_{sij},y_{sij},z_{sij})$	In general, the Cartesian coordinates of the ijth image of the sth source
θ_{sij}	View angle of a light source image subtended by an exit point (x,y)
$\alpha_{si}(\alpha_{sj})$	Angular placement of virtual sources along $x(y)$ direction
H	Lightpipe length
$d_x(d_y)$	Lightpipe input size along $x(y)$ direction
$D_x(D_y)$	Lightpipe output size along $x(y)$ direction
$R_x(R_y)$	Radius of curvature of the array of images along $x(y)$ direction
$\Delta_x(\Delta_y)$	Angle between the pair of pipe walls along $x(y)$ direction
$W1_{sij}(W2_{sij})$	Window functions for the pair of walls along $x(y)$ direction

APPENDIX B: NUMBER OF VISIBLE IMAGES

Not all image sources are visible from the lightpipe output. Only a finite number of images must be considered in the equation for the irradiance spatial distribution. I outline the derivation of such a number in this appendix.

In Eqs. (7a), (7b), (10), and (15) the indices ij are $i=-N_{-x},-(N_{-x}-1),\ldots,-1,0,1,\ldots,(N_{+x}-1),N_{+x}$, and $j=-N_{-y},-(N_{-y}-1),\ldots,-1,0,1,\ldots,(N_{+y}-1),N_{+y}$. Parameter $N_{\pm x}$ is the number of images that are visible along the $\pm x$ direction from the lightpipe output, and $N_{\pm y}$ along the $\pm y$ direction. Two considerations must be made to calculate the number of images: (a) The output point (x,y) that can see the farthest image is at one side, i.e., the point $(x=\pm D_x/2,y=0)$ along the x-direction, and $(x=0,y=\pm D_y/2)$ along the y-direction. (b) The view angle of the last visible image must be less than 90 °, i.e., $\theta_{sij}<90°$. These considerations are illustrated in Fig. 10 for the plane xz. Using Eq. (1), the angle $\alpha_{sN_{+x}}$ along the x-direction is

$$\alpha_{sN_{+x}}=N_{+x}\Delta_x+(-1)^{N_{+x}}\arctan(x_s/R_x).$$

Consideration (b) means that $\alpha_{sN_{+x}}<\alpha_x$, which leads to

$$N_{+x}<\frac{\alpha_x-(-1)^{N_{+x}}\arctan(x_s/R_x)}{\Delta_x}.$$

Because $\alpha_{sN_{+x}}$ is an upper limit, then $\alpha_{s(N_{+x}+1)}>\alpha_x$, which leads to

$$N_{+x}>\frac{\alpha_x+(-1)^{N_{+x}}\arctan(x_s/R_x)}{\Delta_x}-1.$$

And equivalent inequalities can be deduced for N_{-x}.

Finally, again using Eq. (1), for angle α_{s0} it can be noted that $\alpha_{s0}<\Delta_x/2$, which leads to

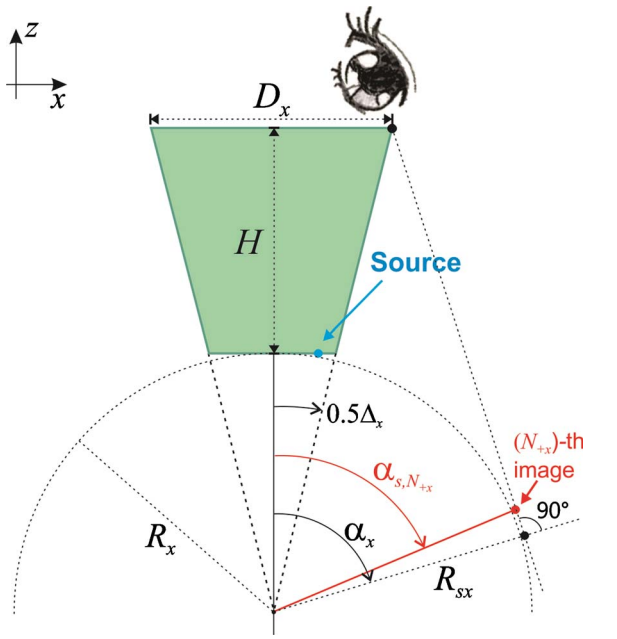

Fig. 10. (Color online) Geometry used to derive the maximum number of visible images $N_{\pm x}$ along x-direction.

$$\frac{\arctan(x_s/R_x)}{\Delta_x}<\frac{1}{2}.$$

After some algebra with these inequalities, it can be deduced that the number of visible images is given by

$$N_{\pm x}=\text{Integer}\left[\frac{\alpha_x\pm(-1)^{Round[\alpha_x/\Delta_x]+1}\arctan(x_s/R_x)}{\Delta_x}\right], \tag{B1}$$

and

$$N_{\pm y}=\text{Integer}\left[\frac{\alpha_y\pm(-1)^{Round[\alpha_y/\Delta_y]+1}\arctan(y_s/R_y)}{\Delta_y}\right], \tag{B2}$$

where

$$\alpha_x=\arccos\left\{\left[\frac{x_s^2+R_x^2}{(H+R_x)^2+D_x^2/4}\right]^{0.5}\right\}+\frac{\Delta_x}{2},$$

$$\alpha_y=\arccos\left\{\left[\frac{y_s^2+R_y^2}{(H+R_y)^2+D_y^2/4}\right]^{0.5}\right\}+\frac{\Delta_y}{2}$$

"Integer[Q]" is the lower integer part of Q; e.g., Integer[7.8]=7. "*Round*[Q]" is Q rounded to the nearest integer. R_x is the curvature radius along the x-direction, and R_y along the y-direction. I verified Eqs. (B1) and (B2) with many numerical computations.

Subsection 3.A includes an additional parameter for the number of visible images through the pair of parallel walls. In theory N is infinitum, but for practical purposes it must be finite. As stated in Section 3, the irradiance due to each image is weighted by the $(|i|+|j|)$th power of the reflectivity ρ of the side walls of the lightpipe. Therefore, I define N as that number that weights the irradiance by a

factor ρ_0; e.g., for images along the y-direction, $\rho^{|i|+|N|}=\rho_0$. The number of images visible along the y-direction, for Eq. (7a) is

$$N = Round\left[\frac{\log \rho_0}{\log \rho}\right] - |i|, \tag{B3}$$

and along the x-direction, for Eq. (7b) is

$$N = Round\left[\frac{\log \rho_0}{\log \rho}\right] - |j|. \tag{B4}$$

In Subsection 3.A a value of $\rho_0=0.1$ was selected to plot Figs. 4 and 5.

REFERENCES

1. F. Fournier, W. J. Cassarly, and J. P. Rolland, "Method to improve spatial uniformity with lightpipes," Opt. Lett. **33**, 1165–1167 (2008).
2. M. Kocifaj, "Analytical solution for daylight transmission via hollow light pipes with a transparent glazing," Sol. Energy **83**, 186–192 (2009).
3. P. D. Swift, R. Lawlor, G. B. Smith, and A. Gentle, "Rectangular-section mirror light pipes," Sol. Energy Mater. Sol. Cells **92**, 969–975 (2008).
4. J. M. Gordon, E. A. Katz, D. Feuermann, and M. Huleihil, "Toward ultrahigh-flux photovoltaic concentration," Appl. Phys. Lett. **84**, 3642–3644 (2004).
5. S. C. Chu and J. L. Chern, "No-loss bent light pipe with an equiangular spiral," Opt. Lett. **30**, 3006–3008 (2005).
6. Y. Qu, J. R. Howell, and O. A. Ezekoye, "Monte Carlo modeling of a light-pipe radiation thermometer," IEEE Trans. Semicond. Manuf. **20**, 39–50 (2007).
7. F. Fournier and J. P. Rolland, "Optimization of freeform lightpipes for light-emitting diode projectors," Appl. Opt. **47**, 957–966 (2008).
8. A. J. W. Whang, P. C. Li, Y. Y. Chen, and S. L. Hsieh, "Guiding light from LED array via tapered light pipe for illumination systems design," J. Disp. Technol. **5**, 104–108 (2009).
9. H. Murat, A. Gielen, and H. De Smet, "Gradually tapered light pipes for illumination of LED projectors," J. Soc. Inf. Disp. **15**, 519–526 (2007).
10. R. Zhang and H. Hua, "8.3: Design of a Compact Light Engine for FLCOS Microdisplays in a p-HMPD System," SID Symposium Digest **39**, 85 –87 (2008).
11. C. M. Cheng and J. L. Chern, "Illuminance formation and color difference of mixed-color light emitting diodes in a rectangular light pipe: an analytical approach," Appl. Opt. **47**, 431–441 (2008).
12. R. Winston, J. C. Miñano, and P. Benítez, *Nonimaging Optics* (Elsevier, 2005).
13. W. Cassarly, "Nonimaging optics: concentration and illumination," in *OSA Handbook of Optics*, 2nd ed., Vol. III (McGraw-Hill, 2001).
14. J. Chaves, *Introduction to Nonimaging Optics* (CRC Press, 2008).
15. A. Gupta, J. Lee, and R. J. Koshel, "Design of efficient lightpipes for illumination by an analytical approach," Appl. Opt. **40**, 3640–3648 (2001).
16. Y.-K. Cheng and J.-L.. Chern, "Irradiance formations in hollow straight light pipes with square and circular shapes," J. Opt. Soc. Am. A, Vol. **23**, 427–434 (2006).
17. M. M. Chen, J. B. Berkowitz-Mattuck, and P. E. Glaser, "The use of a kaleidoscope to obtain uniform flux over a large area in a solar or arc imaging furnace," Appl. Opt. **2**, 265–272 (1963).
18. M. Iona, "Virtual mirrors," Phys. Teach. **20**, 278 (1982).
19. I. Moreno and C. C. Sun, "Modeling the radiation pattern of LEDs," Opt. Express **16**, 1808–1819 (2008).
20. I. Moreno and C. C. Sun, "Three-dimensional measurement of light-emitting diode radiation pattern: a rapid estimation," Meas. Sci. Technol. **20**, 075306 (2009).
21. I. Moreno, J. Muñoz, and R. Ivanov, "Uniform illumination of distant targets using a spherical light-emitting diode array," Opt. Eng. **46**, 033001 (2007).
22. I. Moreno, C. C. Sun, and R. Ivanov, "Far-field condition for light-emitting diode arrays," Appl. Opt. **48**, 1190–1197 (2009).
23. I. Moreno, "Creating a desired lighting pattern with an LED array," Proc. SPIE **7058**, 705811 (2008).